International Journal of Mass Spectrometry and Ion Physics, 29 (1979) 57—75

IONIZATION IN A METHANOL—OXYGEN FLAME

J.M. GOODINGS, CHUN-WAI NG and D.K. BOHME

Department of Chemistry, York University, 4700 Keele Street, Downsview, Ontario M3J 1P3 (Canada)

(Received 1 June 1978)

ABSTRACT

The combustion of methanol was studied in a conical methanol—oxygen flame of fuel-lean composition (equivalence ratio $\phi = 0.25$) burning at atmospheric pressure surrounded by a flowing argon shield. Oxygen bubbled through liquid methanol contained in two gas saturators provided a premixed flame of excellent stability and reproducibility. The flame gas was sampled into a mass spectrometer which was used to detect a variety of naturally occurring ionic species, both positive and negative. Although the maximum level of ionization in this flame had the rather low value of 5×10^8 ions ml^{-1}, nevertheless concentration profiles were drawn as a function of distance along the flame axis at 17 individual mass numbers (m/z) for positive ions and 11 for negative ions; that is, whenever an appreciable signal could be detected below 100 amu. The positive profiles in the reaction zone are dominated by proton transfer processes which indicate that CHO^+ is the primary ion. A variety of protonated combustion intermediates and products were detected including both stable molecules (H_2O, HCHO, the CH_3OH fuel, CH_2CO, CH_3CHO, HCOOH and possibly CH_3OCH_3/C_2H_5OH) and radicals (C, CH, CH_2, HCO, CH_2OH or CH_3O, CH_3CO or CH_2CHO, and possibly CH_3OO). Chemical ionization by charge transfer is certainly operative for two species (O_2 and NO as an impurity) and perhaps others (CH_3, O). As far as the negative ions are concerned, a number of species can be ionized in the reaction zone by three-body electron attachment and subsequent charge transfer processes (O_2 initially, and then O, OH, HO_2, HCOO and possibly HCOOO). Some of these negative ions are sufficiently strong bases to abstract protons from other species in proton transfer reactions (CH_3OH, possibly H_2O_2, HCOOH, and perhaps the peroxidic intermediates HCOOO and HCOOOH). The remaining negative ions detected can be interpreted as cluster ions ($OH^- \cdot H_2O$, $HO_2^- \cdot O_2$ or $HO_2^- \cdot CH_3OH$, $CHO_3^- \cdot H_2O$). All of this ion chemistry was compared with that observed previously for an analogous fuel-lean methane—oxygen flame. Many similarities were noted, particularly downstream, for both positive and negative ions. However, the combustion path leading to formic acid is more prominent in the methanol flame.

INTRODUCTION

The solution to the vanishing supply of retrievable petroleum from the earth's crust will probably involve a considerable variety of other energy sources. Of major interest are those which make use of a renewable or inexhaustible resource. In many parts of the world, fast-growing poplar or syca-

more trees constitute a renewable resource which can readily be used to produce fuel alcohols. The conversion of wood carbohydrates to sugars by enzyme action with subsequent fermentation to ethanol has an overall efficiency of approximately 25% by weight [1]. At the present time in Brazil, up to 20% of cane alcohol is routinely blended with gasoline for use as a motor fuel requiring no carburettor modification [2]. Alternatively, methanol can be obtained from the destructive distillation of wood. Partially oxidized fuels like alcohols offer additional advantages by way of improved pollution and sooting characteristics.

These considerations, and inevitable future interest in alcohols as motor fuels, provided the motivation for the study of a methanol—oxygen flame described here. Considerable information about the underlying neutral chemistry of combustion can be inferred from the ion chemistry of this flame which was observed using the technique of flame-ionization mass spectrometry. Comparisons are made with our similar studies of methane—oxygen flames done previously [3—6]. Information in the literature about methanol flames is sparse. Ignition delay is longer than that for ethanol [7] and flame velocities are similar to those for comparable methane flames [8,9]. Spectroscopic studies have shown the absence of Swan-band emission for C_2 [10]. Kinetic mechanisms have been suggested [7]; in one case, comparisons were made with methane combustion [10].

EXPERIMENTAL

A laminar premixed methanol—oxygen flame was stabilized on a simple cylindrical quartz burner (2.5 mm i.d. × 9.0 mm o.d.) at atmospheric pressure and surrounded by a flowing argon shield. This flame had a moderately bright-blue reaction zone approximately 0.25 mm thick in the form of a cone some 6 mm high and 3 mm in base diameter with a rounded tip. Pure oxygen (CP grade) with a volume flow rate $\dot{V}_1 = 17.0$ ml s^{-1} measured at 298 K and typical room atmospheric pressure $P_{atm} = 740$ torr was passed through two gas saturators in series containing methanol (analytical reagent grade), each followed by a commercially available flash arrestor (Matheson 6103) as shown in Fig. 1. Except for the second flash arrestor, all of this equipment was submerged in a stirred water bath with the second saturator maintained at 296.2 ± 0.3 K such that the saturation vapour pressure of methanol P^0_M could be maintained at 111 ± 2 torr. Additional pure oxygen with a typical flow rate $\dot{V}_2 = 1.0$ ml s^{-1} at 298 K and 740 torr was added downstream to provide a fuel-lean combustible mixture of equivalence ratio $\phi = 0.250$ for the typical figures given above, calculated from the formula

$$\phi = (\tfrac{3}{2})[P^0_M/(P_{atm} - P^0_M)][\dot{V}_1/(\dot{V}_1 + \dot{V}_2)] \quad (1)$$

where the effective methanol flow rate $\dot{V}_M$ is 3.00 ml s^{-1} at 298 K and 740 torr from

$$\dot{V}_M = \dot{V}_1 P^0_M/(P_{atm} - P^0_M) \quad (2)$$

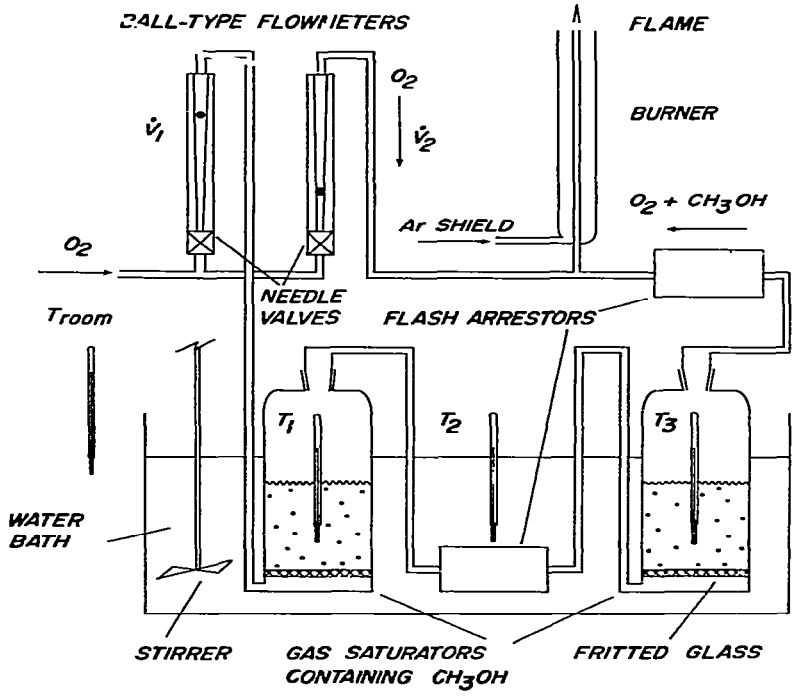

Fig. 1. Premixed methanol—oxygen supply to the burner. The operating temperatures are $T_{room} > 298$ K, $T_1 = 295.2$ K, $T_2 = 295.7$ K and $T_3 = 296.2$ K; variations of T_1, T_2 and T_3 are each $< \pm 0.3$ K.

For variations in room atmospheric pressure from day to day, ϕ was nevertheless maintained at 0.250 by appropriate changes to $\dot{V}_2$; that is, the input mole fractions of methanol and oxygen were maintained at 0.143 and 0.857, respectively. A computer programme (GASTEMP, Shell Research Limited) based on JANAF Thermochemical Tables [11] was used to calculate the adiabatic flame temperature of 2377 K and the corresponding equilibrium burnt gas composition given in Table 1.

It was noted repeatedly that the premixed gas would not ignite with a match for $\phi < 0.245$. Therefore, it was just possible to operate a stable flame near this flammability limit in a reasonably safe manner without resorting to heated burner and burner tubes. A sufficient saturation vapour pressure P_M^0 was obtainable at 296.2 K for $\phi = 0.250$. For safety, however, the laboratory temperature was always maintained above 298 K so that methanol could never condense anywhere in the second flash arrestor, burner tubes or burner. Since the flame velocity of this fuel-lean flame will increase with increasing methanol concentration, any condensation of methanol must be avoided since it would promote a dangerous flash-back condition. It is particularly important in a set-up of this kind involving gas saturators since the

TABLE 1

Calculated equilibrium burnt gas composition

Species	Mole fraction
O_2	0.588
H_2O	0.253
CO_2	0.129
OH	0.0199
O	0.00591
CO	0.00312
H_2	0.00106
H	4.68×10^{-4}
HO_2	1.91×10^{-5}
O_3	9.26×10^{-8}
HCO	3.75×10^{-9}

volume of explosive premixed methanol—oxygen gas is inevitably rather large (ca. 800 ml). For added safety, each saturator was protected with its own flash arrestor. The two efficient saturators shown in Fig. 1, fitted with fritted glass discs 7 cm in diameter which produce large numbers of small bubbles, were sufficient to guarantee saturation of the oxygen stream at 296.2 K; the loss of methanol from the second saturator is less than 1 g h^{-1} compared with more than 13 g h^{-1} from the first saturator.

The simple burner shown in Fig. 1 was mounted on a motor-driven carriage having accurate axial alignment and calibrated drive such that 0.1 mm along the flame axis corresponded to 1 cm on the X-axis of an X-Y recorder. Details of the flame-ion mass spectrometer have been given previously [3,6]. Very briefly, the flame burned vertically upwards against a pinhole 0.09 mm in diameter in a platinum—iridium disc welded into a water-cooled stainless steel flange. The sampling rate was approximately 1 ml s^{-1} at room temperature and pressure. The gas sample passed into a first vacuum chamber maintained near 10^{-4} torr by a fast vapour booster pump. The ions were focussed electrostatically through a 2-mm orifice into a second vacuum chamber maintained below 8×10^{-6} torr by a 6-in. diffusion pump and liquid nitrogen trap. The ion beam was analyzed by a 6-in. quadrupole mass filter. The transmitted ion current was collected on a Faraday cage, amplified by a vibrating reed electrometer (grid leak resistance of 10^{11} Ω) and displayed on the Y-axis of the X-Y recorder. Thus, the fundamental data consisted of profiles of ion signal (in mV) for individual ionic species versus distance along the flame axis, z. Positive or negative ions could be detected by reversing the polarity on all electrodes.

Calibration measurements have shown that approximately 20% of the ions entering the sampling pinhole reach the mass filter. Profiles could be drawn for ionic species having maximum concentrations in the reaction zone as small as 5×10^5 ions ml^{-1}. Simultaneously with the tracing of each ion pro-

file, the flame pressure profile derived from an ionization gauge in the second vacuum chamber was drawn on a second X-Y recorder. The pressure profile showed a sharp bend corresponding to the downstream tip of the luminous reaction zone, and provided a reproducible origin ($z = 0$) in the flame for the distance scale of the ion profiles.

RESULTS AND DISCUSSION

Spurious ion profiles from flash arrestors

Before going any farther, it is worth mentioning a troublesome phenomenon which may be encountered by other workers. The commercially available flash arrestors (Matheson 6103) contain a spring-loaded check valve followed by a small-diameter copper cooling coil. For gas flow rates >10 standard ml s^{-1} (up to the highest values used of 30 ml s^{-1}), the check valve gave rise to stable oscillations in the frequency range 250—500 Hz depending on the flow rate. The frequency is easily ascertained from the pitch of the musical note heard when a length of tubing connected to the flash arrestor is placed near the experimenter's ear. Both flash arrestors exhibited similar behaviour.

The effect on the ion profiles was dramatic. Figure 2 shows CHO_2^- profiles at 45 amu traced minutes apart with, and without, oscillations at 440

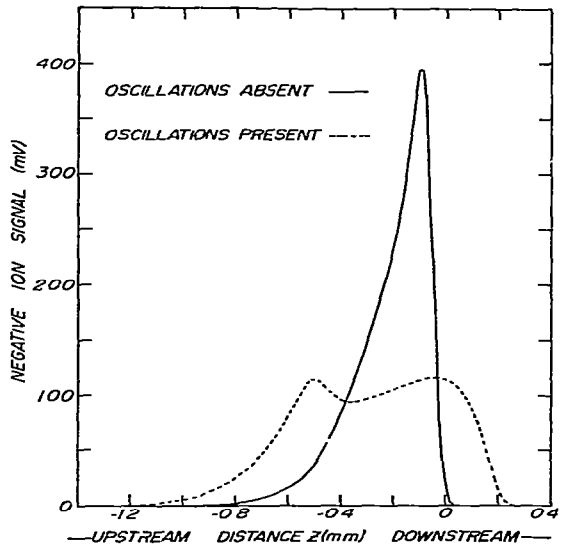

Fig. 2. The effect on a typical flame-ion profile of oscillations in the second flash arrestor. The same negative ion profile at 45 amu is shown with oscillations at 440 Hz both present (dashed curve) and absent (solid curve).

Hz in the second flash arrestor. When present, pressure pulses from the oscillations were transmitted through the gas from the flash arrestor to the flame through the interconnecting tubing where their presence was just discernible to the eye as a slight fuzziness of the inner bright luminous zone. The effect was to spread out the reaction zone in space. The double-peaked structure is expected; the oscillating reaction zone spends more time near its turning points than in the middle. The distance between the two peaks has been observed anywhere in the range 0.2—0.8 mm. In Fig. 2, the integrated ion signals represented by the areas under the two curves are approximately equal. Similar curves were obtained at virtually every mass number where ion signals could be observed.

We were able to find spatial orientations of these flash arrestors where the oscillations did not occur if the gas flow was started slowly. Once started, however, the oscillations would proceed indefinitely and were difficult to detect. We draw the attention of other workers to this potential problem since it could easily go undetected while possibly having a deleterious effect.

Total ionization profiles

Before presenting data for individual ionic species, some considerations of total ion profiles provide a useful background to the discussion. Total positive and negative ion profiles are given in Fig. 3, and bear a strong qualitative resemblance to those obtained for a fuel-lean methane—oxygen flame [4]. As mentioned earlier, the reaction zone extended upstream from $z = 0$ although the distance scale was distorted in this region because of the conical flame geometry. That is, the thickness of the reaction zone through the side of the

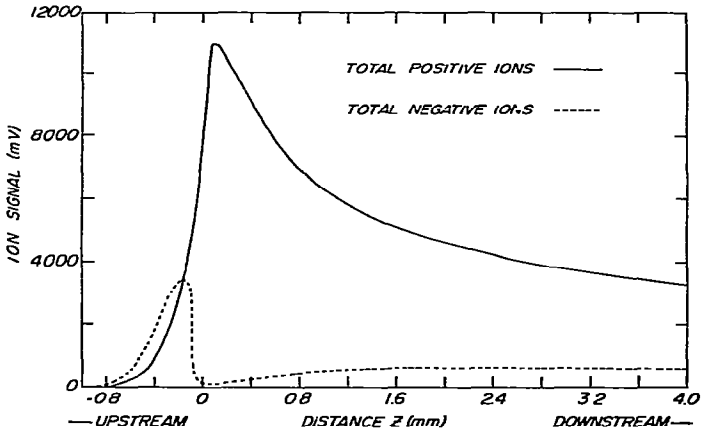

Fig. 3. Total ionization profiles for both positive ions (solid curve) and negative ions (dashed curve).

bright luminous cone was approximately 0.25 mm. It appears much larger when sampling along the flame axis, however. With the mass-spectrometric sampling probe inserted well upstream of $z = 0$, ions can still diffuse through the sampling orifice from the inside surface of the truncated luminous cone. Also, the negative ion profile extends upstream of its positive ion counterpart in the same manner noted previously [4]. Free electrons from the primary chemi-ionization process have a high mobility and can diffuse upstream of the positive ions against the flow by an amount which depends on the Debye length for the flame plasma in this region; a more detailed consideration of the phenomenon is underway in our laboratory.

The ion density $[I^+]$ at a point in the flame was estimated from the total collection of positive ions on lens elements in the first vacuum chamber divided by the volume flow rate through the sampling orifice. At the peak of the positive ion profile, $[I^+]$ was estimated to be 5×10^8 ions ml^{-1} at the flame temperature where the total gas density is 3×10^{18} ml^{-1}. This amount of ionization is rather low compared with a peak density approximately three times as large measured in a similar fuel-lean methane—oxygen flame [4,6]. The ratio for these two fuels is in excellent agreement with that measured by Bulewicz and Padley [12], whose results show that the partially oxidized alcohol fuel has a lesser tendency than the corresponding hydrocarbon to decompose to form CH radicals. The last statement assumes that ions originate primarily by the chemi-ionization process [12—14]

$$CH + O \rightarrow CHO^+ + e^- \quad \Delta H^0 = -17 \qquad (3)$$

whose rate in a flame is probably limited by the production of CH rather than O atoms. (Empirical formulae for ions will be used throughout, but structural formulae for neutrals to avoid isomeric ambiguities. Standard heats of reaction ΔH^0 are quoted at 298 K in kJ mol^{-1}.)

Figure 3 also shows that negative ions achieve a maximum concentration in the reaction zone just less than one-third of the maximum value for positive ions. Downstream, the negative ion concentration is surprisingly constant while the positive ions decrease; that is, $[I^-]/[I^+]$ increases steadily over a range of several mm. This implies that the net loss of negative ions through ion—ion recombination, associative detachment and collisional detachment is small compared with the net loss of positive ions through electron—ion recombination.

Intermediates in the oxidation/pyrolysis of methanol

Many oxidation studies of fuels have been carried out at comparatively low temperatures in the range 500—1000 K in glass vessels. In general, flames burn at considerably higher temperatures without contributions from wall reactions. In a premixed flame when unburnt fuel approaches the reaction zone, it suffers a rapid temperature increase before maximum temperature is reached, and some pyrolysis may precede the actual oxidation processes.

Even in a fuel-lean flame, large quantities of oxygen may have only a small effect on the initial pyrolytic decomposition [15].

A considerable body of evidence [16—18] suggests that methanol is initially converted to formaldehyde by reactions possibly involving methyl peroxide as an intermediate

$$CH_3OH + O_2 \rightarrow CH_3OO + OH \qquad \Delta H^0 = +268 \qquad (4)$$

$$CH_3OO + M \rightarrow HCHO + OH + M \qquad \Delta H^0 = -96.9 \qquad (5)$$

or CH_2OH and HO_2 radicals

$$CH_3OH + O_2 \rightarrow CH_2OH + HO_2 \qquad \Delta H^0 = +204 \qquad (6)$$

$$CH_2OH + O_2 \rightarrow HCHO + HO_2 \qquad \Delta H^0 = -70 \qquad (7)$$

Reactions similar to the last two involving H-atom abstraction by OH, H or HO_2 would give rise to H_2O, H_2 and H_2O_2, respectively, as intermediates.

The oxidation of formaldehyde has been considered in a number of reviews [19—21]. At flame temperatures, the major loss of formaldehyde should involve H-atom abstraction to form formyl radicals, either in a chain-branching reaction with oxygen

$$HCHO + O_2 \rightarrow HCO + HO_2 \qquad \Delta H^0 = +173 \qquad (8)$$

or by radical attack

$$HCHO + X \rightarrow HCO + HX \qquad (9)$$

where X is OH, H or HO_2, as mentioned above. In a similar manner, formyl radicals should be lost by further H-atom abstraction

$$HCO + O_2 \rightarrow CO + HO_2 \qquad \Delta H^0 = -133 \qquad (10)$$

which has a low activation energy [19] and is therefore preferred over thermal decomposition

$$HCO + M \rightarrow H + CO + M \qquad \Delta H^0 = +64.0 \qquad (11)$$

or association

$$HCO + O_2 \rightarrow HCO_3 \qquad (12)$$

Although peroxidic compounds like HCO_3 might not be expected to play a major role at flame temperatures, they should be mentioned since they are dominant in certain low-temperature mechanisms. The key species is performic acid

$$HCHO + O_2 \rightarrow HCOOOH \qquad (13)$$

$$HCHO + HCO_3 \rightarrow HCO + HCOOOH \qquad (14)$$

which may have a variety of decomposition products

$$HCOOOH \rightarrow HCO + HO_2 \quad (15a)$$

$$\rightarrow HCOO + OH \quad (15b)$$

$$\rightarrow CO + H_2O_2 \quad (15c)$$

$$\rightarrow HCOOH + O \quad (15d)$$

As an alternative to eqn. (15d) for the production of formic acid, Hay and Hessam [22] postulated a source reaction involving HO_2 radicals

$$HCHO + HO_2 \rightarrow HCOOH + OH \qquad \Delta H^0 = -251 \quad (16)$$

It is unnecessary to list here the various chain termination reactions. Of major interest, however, is the variety of neutral intermediate species which may undergo chemical ionization in the flame and subsequent detection in the flame-ion mass spectrometer. In order of increasing molecular weight, these include H, O, OH, H_2O, CO, HCO, HCHO, CH_2OH (or CH_3O), CH_3OH, O_2, HO_2, H_2O_2, CO_2, HCOO, HCOOH, CH_3OO, HCO_3 and HCOOOH.

Positive ion profiles

Individual ion profiles were recorded at every mass number below 100 amu where an appreciable signal could be detected. In this way, a family of profiles was obtained at 17 mass numbers for positive ions and 11 for negative ions. These figures do not include a number of profiles clearly attributable to isotopic species involving ^{13}C, D, ^{17}O and ^{18}O. The positive ion profiles are shown in Figs. 4—6. Figure 4 presents species whose signals persist downstream into the burnt gas including H_3O^+ and its first two hydrates; in addition, the signals at 32 and 16 amu have peaks in the reaction zone ($z <$

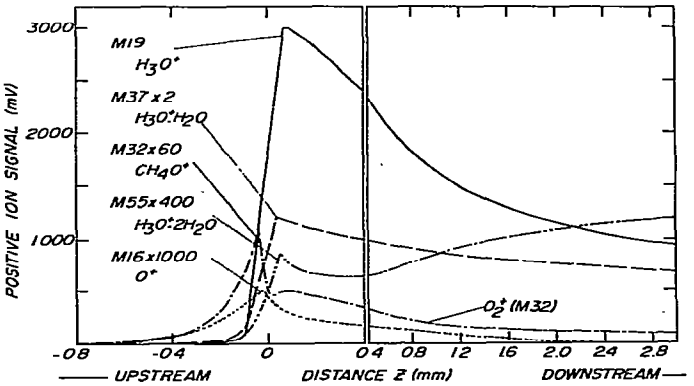

Fig. 4. Positive ion profiles which persist downstream into the burnt gas.

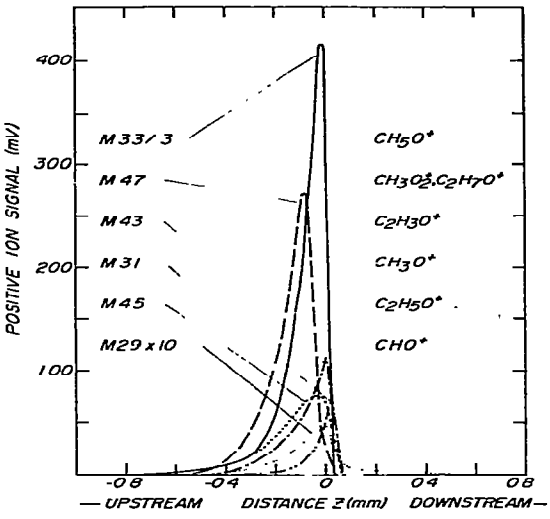

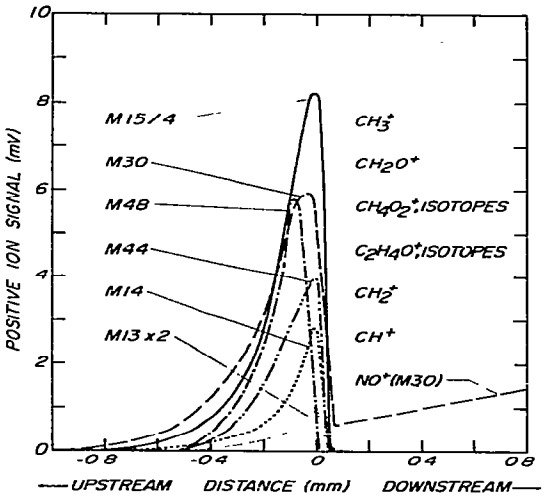

Fig. 5. Positive ion profiles arising from the protonation of stable molecular species in the reaction zone.

Fig. 6. Positive ion profiles arising from the protonation of radical species in the reaction zone.

0). The remaining peaks in Figs. 5 and 6 are confined to the reaction zone and conveniently divide into two groups on a basis of size. It will become apparent that the large signals of Fig. 5 are due to protonated stable neutrals while the small signals of Fig. 6 arise mainly from protonated radicals. Assignments for the mass numbers m/z of these ions are given in Table 2 together with the corresponding neutral species from which the ions are likely to be formed and the probable chemical ionization processes. Most of the ions in Table 2 are consistent with the presence in the flame of expected neutral intermediates. However, additional comment is warranted in some cases and will be given in order of increasing mass number.

The CH^+, CH_2^+ and CH_3^+ profiles shown in Fig. 6 may arise from proton transfer to C, CH and CH_2 radicals, respectively. The low ionization energy for CH_3 of 9.76 eV at 298 K means that a contribution to the CH_3^+ profile may stem from charge transfer to CH_3 radicals. A reasonable mechanism for the formation of the CH_x (x = 1—3) radicals might be the thermal decomposition of methyl peroxide different from that given in eqn. (5)

$$CH_3OO + M \rightarrow CH_3 + O_2 + M \qquad \Delta H^0 = +118 \qquad (17)$$

followed by sequential H-atom abstraction

$$CH_x (x = 3—1) + OH \rightarrow CH_{x-1} + H_2O \qquad (18)$$

In any event, the presence of CH_x^+ (x = 1—3) profiles provides evidence for a

TABLE 2

Mass numbers and assignments of positive ions

Mass number (amu)	Empirical formula	Corresponding neutral	Probable mechanism
13	CH^+	C	Proton transfer
14	CH_2^+	CH	Proton transfer
15	CH_3^+	CH_2, CH_3	Proton transfer, charge transfer
16	O^+	O, O_2	Charge transfer, rearrangement
19	H_3O^+	H_2O	Proton transfer
29	CHO^+	CH + O, see text	Chemi-ionization
30 upstream	CH_2O^+	HCO	Proton transfer
downstream	NO^+	NO	Charge transfer
31	CH_3O^+	HCHO	Proton transfer
32 upstream	CH_4O^+	CH_2OH, CH_3O	Proton transfer
downstream	O_2^+	O_2	Charge transfer
33	CH_5O^+	CH_3OH	Proton transfer
37	$H_3O^+ \cdot H_2O$	H_2O	Clustering
43	$C_2H_3O^+$	CH_2CO	Proton transfer
44	$C_2H_4O^+$, isotopes	CH_3CO	Proton transfer
45	$C_2H_5O^+$	CH_3CHO	Proton transfer
47	$CH_3O_2^+$, $C_2H_7O^+$	HCOOH, CH_3OCH_3	Proton transfer
48	$CH_4O_2^+$, isotopes	CH_3OO, see text	Proton transfer
55	$H_3O^+ \cdot (H_2O)_2$	H_2O	Clustering

secondary combustion path at flame temperatures which is different from the expected CH_3OH—HCHO—HCO—CO path.

Formation of CH_4^+ at 16 amu is not expected, however, since the proton affinity *PA* of CH_3 has the very low value of 536 ± 8 kJ mol^{-1} [11,6], and CH_4 is not present to take part in a charge transfer reaction. If this is the case, the smallest profile in Fig. 4 at 16 amu must arise from O^+. This profile is remarkably similar to one observed in a fuel-lean methane—oxygen flame [3], and may stem from a known secondary channel of the reaction of CH^+ with oxygen [23]

$$CH^+ + O_2 \rightarrow O^+ + HCO \qquad \Delta H^0 = -18 \qquad (19)$$

In general, the high heat of formation of O^+ equal to 1565 kJ mol^{-1} at 298 K makes source reactions difficult to postulate although loss reactions are rather numerous (see Fig. 6 of ref. 3).

The smallest profile in Fig. 5 at 29 amu which peaks in the reaction zone and then persists to some extent downstream can only be due to CHO^+ ions. These may be formed by the chemi-ionization reaction (3), by proton transfer to CO whose *PA* has the low value of 596.6 ± 4.2 kJ mol^{-1} at 298 K [24,6]

$$HX^+ + CO \rightarrow CHO^+ + X \qquad (20)$$

by charge transfer to HCO whose ionization energy is only 8.13 eV at 298 K [24,11]

$$Y^+ + HCO \rightarrow CHO^+ + Y \qquad (21)$$

or by other ion—molecule reactions involving heavy particle rearrangement such as the hydride ion transfer reaction

$$CH_3^+ + HCHO \rightarrow CHO^+ + CH_4 \qquad \Delta H^0 = -226 \qquad (22)$$

which has a fast rate constant $k = (1.00 \pm 0.05) \times 10^{-9}$ ml molecule^{-1} s^{-1} at 298 K [25]. The contribution of reaction (20) will be negligible since the concentration of CO will be low early in the reaction zone and ionic species HX^+ corresponding to neutrals X having *PA*s less than that of CO (e.g. CO_2, CH_3, O_2, O, H_2) were not detected. The charge transfer production of CHO^+ by reaction (21) is difficult to assess. Many of the ions observed in this region have energies sufficient to ionize HCO (e.g. Y^+ equal to CH^+, CH_2^+, CH_3^+, O^+, CH_2O^+, O_2^+, etc.) although the nature of their reactions with HCO is unknown. Other ion—molecule reactions may contribute to the CHO^+ signal in varying degrees. Certainly the contribution of eqn. (22) to the CHO^+ signal will become appreciable if the peak concentration of HCHO becomes large. Downstream, CHO^+ may be produced by proton transfer via the backward reaction of

$$CHO^+ + H_2O \rightleftharpoons H_3O^+ + CO \qquad \Delta H^0(\text{forward}) = -95 \qquad (23)$$

involving a very large ion signal H_3O^+ and a sizeable neutral concentration for CO; the viability of this process has been demonstrated previously [5]. Loss processes for CHO^+ have already been considered in some detail [3,6] and are not expected to differ appreciably in this flame. In particular, the role of CHO^+ as an initiator of sequential proton transfer reactions which dominate the ion chemistry in the reaction zone has been emphasized.

The small rising signal downstream at 30 amu in Fig. 6 undoubtedly comes from charge transfer to NO formed when room air is entrained into the burnt gas through the argon shield. Although most of the signal at 31 amu can probably be ascribed to protonated formaldehyde, there are fast reactions involving CH_x^+ ($x = 3$—1) with methanol [26] which can also lead to this ion such as

$$CH_3^+ + CH_3OH \rightarrow CH_3O^+ + CH_4 \qquad \Delta H^0 = -247 \qquad (24)$$

For the sharp upstream peak of the profile at 32 amu in Fig. 4, presumably protonated CH_2OH (or CH_3O) radicals make a major contribution. The downstream peak occurs in approximate coincidence with the profile maxima for H_3O^+ and its hydrates, and the signal then continues on far downstream. The behaviour can be explained by O_2^+ in equilibrium with H_3O^+

making use of a reaction sequence

$$H_3O^+ + OH \rightleftharpoons H_2O^+ + H_2O \qquad \Delta H^0 = +91 \tag{25a}$$

$$H_2O^+ + O_2 \rightleftharpoons O_2^+ + H_2O \qquad \Delta H^0 = -54 \tag{25b}$$

$$H_3O^+ + O_2 + OH \rightleftharpoons O_2^+ + 2\,H_2O \qquad \Delta G^0_{2300} = +46 \tag{25}$$

invoked previously for a fuel-lean methane—oxygen flame [3].

No positive-ion evidence was found for either HO_2 or H_2O_2 even though the condition $PA(CO) < PA(HO_2)$, $PA(H_2O_2) < PA(HCO)$ (see Table 1 in ref. 6) would be favorable for their detection. Profiles observed at 34 and 35 amu were entirely accounted for by isotopic contributions from CH_5O^+; at 35 amu, the relevant species is $CH_5{}^{18}O^+$. Profiles for the first and second hydrates of H_3O^+ at 37 and 55 amu are shown separately in Fig. 4 although they probably form mainly during passage through the cold boundary layer and expansion cooling at the sampling orifice [27].

Profiles at mass numbers 43, 44 and 45 are not surprising when exothermic reactions of radicals like CH_x ($x = 0$—3), HCO and CH_2OH with major stable neutrals such as CH_3OH and HCHO are considered. Examples might be

$$CH_2 + HCHO \rightarrow CH_2CO + H_2 \qquad \Delta H^0 = -339 \tag{26}$$

$$HCO + CH_3OH \rightarrow CH_3CO + H_2O \qquad \Delta H^0 = -107 \tag{27}$$

$$CH_2OH + HCHO \rightarrow CH_3CHO + OH \qquad \Delta H^0 = -0.3 \tag{28}$$

Certainly CH_2CO and CH_3CHO, and presumably CH_3CO also, possess high *PA* values (see Table 1 in ref. 6) and will readily undergo chemical ionization in proton transfer reactions [28]. The detection of these species probably reflects their high *PA* values rather than high concentrations. Nevertheless, they provide evidence for the existence of neutral condensation reactions not included in the neutral reaction scheme discussed previously.

The second largest profile in the reaction zone is at 47 amu shown in Fig. 5 and is the first to reach a maximum upstream. The logical candidate is $CH_3O_2^+$ formed by proton transfer to formic acid which has a high *PA* value [29,6] and may be produced in reactions like (16d) and (17). A possible, albeit less likely, alternative is $C_2H_7O^+$ arising from proton transfer to CH_3OCH_3 or C_2H_5OH, both of which have a *PA* value even higher than that of HCOOH [29,6]. Proton transfer from CHO^+ to all three species has been studied recently with the York flowing afterglow apparatus which, in the case of C_2H_5OH, was accompanied by dissociation at room temperature [28]

$$C_2H_7O^+ \rightarrow H_3O^+ + C_2H_4 \qquad \Delta H^0 = +136 \tag{29}$$

Possible source reactions for these C_2H_6O compounds in the flame

$$CH_3OH + CH_3 \rightarrow CH_3OCH_3 + H \qquad \Delta H^0 = +88.92 \tag{30a}$$

$$\rightarrow C_2H_5OH + H \qquad \Delta H^0 = +37.88 \tag{30b}$$

tend to be endothermic at 298 K. One of these compounds may be involved in the downstream foot of the profile at 47 amu. This peculiar feature has also been observed previously for a fuel-lean methane—oxygen flame [3].

However, the profile at 48 amu shown in Fig. 6 also occurs early in the reaction zone and would be entirely accounted for by isotopic contributions from $C_2H_7O^+$ (primarily $^{13}C^{12}CH_7O^+$). On the other hand, if formic acid is involved, only about one-half of the profile at 48 amu would be due to $^{13}CH_3O_2^+$. The logical candidate for the remaining half would be protonated CH_3OO radicals which should occur early in the reaction zone. Although not conclusive, the explanation for the profiles at 47 and 48 amu involving HCOOH and CH_3OO is more in keeping with the expected neutral flame chemistry.

A summary of positive-ion results is given in the final section on conclusions. At this stage, however, it must be apparent that most of the ionic species in Table 2 stem from chemical ionization of many of the expected neutral flame species listed at the end of the preceding section.

Negative ion profiles

Individual negative ion profiles are given in Figs. 7 and 8. Each of the five profiles in Fig. 7 has a sharp maximum in the reaction zone and persists far downstream where it shows a second broad maximum or plateau; for the OH^- profile only, a third small peak is evident between the two maxima. Each of the six profiles in Fig. 8 has a single sharp maximum in the reaction zone and the signal falls rapidly to zero near $z = 0$ on the distance axis. In addition to these eleven profiles, there are a number of tiny signals (<1 mV) particularly at the higher mass numbers which, although clearly detectable, have a signal-to-noise ratio too small for the measurement of meaningful pro-

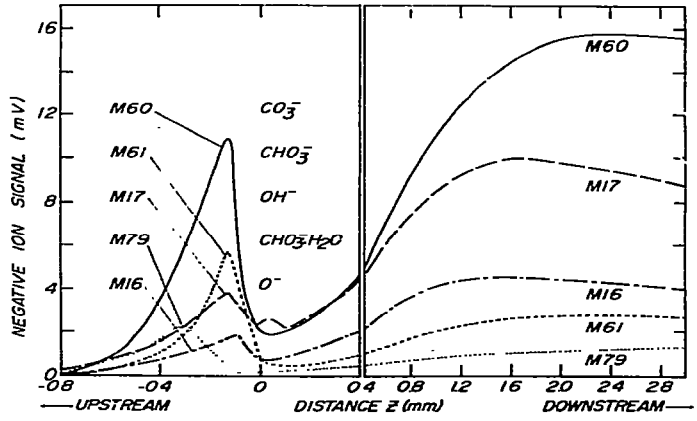

Fig. 7. Negative ion profiles which persist downstream into the burnt gas.

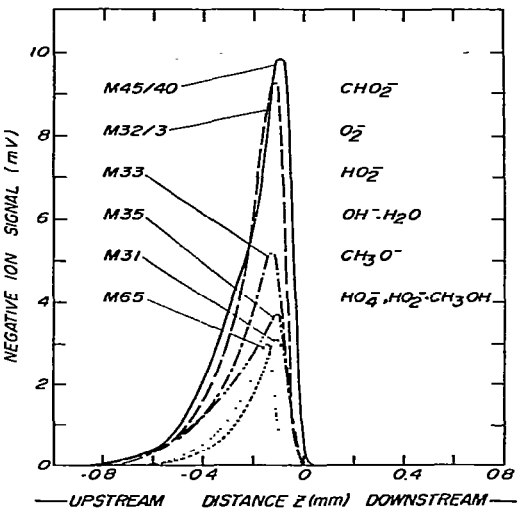

Fig. 8. Negative ion profiles which are confined to the reaction zone.

files. Assignments for the mass numbers of the 11 ionic species are given in Table 3 together with their corresponding neutrals and the probable chemical ionization processes.

The case has been made previously [4] that O_2^- is the first negative ion formed by three-body electron attachment to O_2^-. Charge transfer from O_2^- to O and OH will be exothermic at all temperatures although direct electron attachment is also possible. These processes will be operative both upstream

TABLE 3

Mass numbers and assignments of negative ions

Mass number (amu)	Epirical formula	Corresponding neutral	Probable mechanism
16	O^-	O	Charge transfer, attachment
17	OH^-	OH	Charge transfer, attachment
31	CH_3O^-	CH_3OH	Proton transfer
32	O_2^-	O_2	Attachment
33	HO_2^-	HO_2, H_2O_2	Charge transfer, proton transfer
35	$OH^- \cdot H_2O$	H_2O	Clustering
45	CHO_2^-	HCOOH	Proton transfer
60	CO_3^-	HCOOO, see text	Proton transfer, etc.
61	CHO_3^-	HCOOOH, see text	Proton transfer, etc.
65	$HO_2^- \cdot O_2$, $HO_2^- \cdot CH_3OH$	O_2, CH_3OH	Clustering
79	$CHO_3^- \cdot H_2O$	H_2O	Clustering

in the reaction zone as well as downstream in the burnt gas. Direct electron attachment may also be responsible for the small intermediate peak in the OH^- profile just downstream of $z = 0$. This intermediate peak occurs in approximate coincidence with the sharp maxima in the H_3O^+ and its hydrate profiles. These maxima correspond to a maximum in the free electron concentration as is evident in Fig. 3.

Proton transfer involving the abstraction of protons from methyl alcohol by basic anions

$$OH^- + CH_3OH \rightarrow CH_3O^- + H_2O \qquad \Delta H^0 = -42 \tag{31}$$

$$O^- + CH_3OH \rightarrow CH_3O^- + OH \qquad \Delta H^0 = -5 \tag{32}$$

probably outweighs attachment to CH_2OH (or CH_3O) radicals because of the very high concentration of CH_3OH. The case is less clear for the profile at 33 amu in Fig. 8, however, since both HO_2 and H_2O_2 might well be involved

$$e^- + HO_2 + M \rightarrow HO_2^- + M \qquad \Delta H^0 = -297 \tag{33}$$

$$O_2^- + HO_2 \rightarrow HO_2^- + O_2 \qquad \Delta H^0 = -249 \tag{34}$$

$$OH^- + H_2O_2 \rightarrow HO_2^- + H_2O \qquad \Delta H^0 = -239 \tag{35}$$

In either event, the profile provides some evidence for a neutral species which is not forthcoming from the positive ion data. The peak at 35 amu, which can only be due to the $OH^- \cdot H_2O$ hydrate, is slightly larger than the OH^- peak although most of the hydrate may form during sampling [27]. Unlike OH^-, the hydrate is not observed downstream, however. The largest negative-ion signal at 45 amu undoubtedly stems from the fact [4,6] that HCOOH is a sufficiently strong acid such that proton abstraction by even the very weak base O_2^- is exothermic

$$O_2^- + HCOOH \rightarrow CHO_2^- + HO_2 \qquad \Delta H^0 = -36 \tag{36}$$

A number of source reactions for CO_3^- and CHO_3^- have been suggested previously for a methane—oxygen flame including direct reaction with CHO_2^-, fast switching reactions of hydrated cluster ions and three-body association reactions involving CO and CO_2 [4,6]. Also, it was pointed out that the two ions might equilibrate rapidly by a reaction such as

$$CHO_3^- + OH \rightleftharpoons CO_3^- + H_2O \tag{37}$$

In the reaction zone of this methanol—oxygen flame, however, certain neutral peroxidic compounds mentioned in eqns. (12)—(15) might provide additional sources of these ions

$$OH^- + HCOOOH \rightarrow HCO_3^- + H_2O \tag{38}$$

$$OH^- + HCO_3 \rightarrow CO_3^- + H_2O \tag{39}$$

Downstream, the late broad maxima in the profiles near $z = 2.3$ mm at 60

and 61 amu implies the involvement of CO_2. For example, the hydrated OH observed in the reaction zone might take part in a switching reaction

$$OH^- \cdot H_2O + CO_2 \rightarrow OH^- \cdot CO_2 + H_2O \quad (40)$$

where the product ion could rearrange to form the highly stable HCO_3^- bicarbonate ion [30]. Subsequent water clustering to form $HCO_3^- \cdot H_2O$ would account for the small profile measured at 79 amu. A similar profile at 78 amu attributable to $CO_3^- \cdot H_2O$ is apparently below the limit of detection. Finally, cluster ions arising from three-body association reactions with HO_2^- could account for the profile which peaks early in the reaction zone at 65 amu

$$HO_2^- + CH_3OH + M \rightarrow HO_2^- \cdot CH_3OH + M \quad (41)$$

$$HO_2^- + O_2 + M \rightarrow HO_4^- + M \quad (42)$$

The negative-ion results will be summarized in the final section on conclusions.

Comparison of fuel-lean methanol and methane flames

In many respects, the families of positive and negative ion profiles given in Figs. 4—8 are remarkably similar to those measured previously for a fuel-lean methane—oxygen flame [3,4,6]. Although the level of ionization is less for the methanol flame, the relative profile heights for positive ions in the reaction zone decrease in order of mass numbers 33, 47, 43, 31, 45, 15 amu, etc. (see Figs. 4—6) compared with 43, 33, 47, 31, 45, 15 amu, etc. for the methane flame. That protonated methanol at 33 amu is enhanced in the methanol flame is hardly surprising. In other respects, the signal at 47 amu is enhanced while that at 43 amu is greatly diminished, emphasizing a decomposition channel in the methanol flame involving HCOOH rather than CH_2CO. In addition to magnitudes, the profile positions in the two flames are strikingly similar. For example, the profile at 47 amu peaks furthest upstream while that at 31 amu peaks furthest downstream in the reaction zone.

For negative ions, profiles are detected at most of the same mass numbers in the reaction zone of the two flames although the relative magnitudes differ to some extent. Perhaps the most outstanding feature of the methanol flame is the degree to which the HCO_2^- peak at 45 amu dominates, being more than five times as large as the sum of the profile magnitudes at all other mass numbers in the reaction zone. Once again, as was the case with positive ions, formic acid is emphasized as an intermediate. In fact, starting with the methanol fuel molecule containing oxygen, formic acid is a reasonable product for a combustion path such as

$$CH_3OH \xrightarrow{R} RH + CH_2OH \xrightarrow{O_2} OOCH_2OH \xrightarrow{M} OH + HCOOH$$

commencing with H-atom abstraction by a species R. A parallel combustion

path for methane

$$CH_4 \xrightarrow{R} RH + CH_3 \xrightarrow{O_2} CH_3OO \xrightarrow{M} OH + HCHO$$

results in formaldehyde rather than formic acid. Finally, the downstream behaviour in the burnt gas for both positive and negative ions is very similar for the methanol and methane flames as expected since the chemical identity of the fuel will not survive so far downstream.

CONCLUSIONS

This fuel-lean ($\phi = 0.250$) methanol—oxygen flame has a level of ionization of just 5×10^8 ions ml^{-1}, lower by a factor of three than that for a methane—oxygen flame of even more fuel-lean composition ($\phi = 0.21$) studied previously [3,4,6]. To a considerable degree, the positive-ion chemistry in the reaction zone is dominated by proton transfer reactions. This model supports the designation of CHO^+ as the primary ion. Chemical ionization by proton transfer indicates the presence of a number of combustion intermediates and products, both stable molecules (H_2O, CO, HCHO, CH_2CO, CH_3CHO, HCOOH or CH_3OCH_3/C_2H_5OH) and unstable species including radicals (C, CH, CH_2, HCO, CH_2OH or CH_3O, CH_3CO or CH_2CHO, and possibly CH_3OO). Chemical ionization by charge transfer is certainly operative for two species (NO, O_2) and may be involved in other cases (CH_3, O). However, the positive ions do not provide any clear-cut evidence for peroxidic compounds.

With regard to the negative ions, a variety of chemical ionization processes are operative. Three-body electron attachment to O_2 makes O_2^- the primary ion which can charge-transfer to a variety of radical species of higher electron affinity (O, OH, HO_2, HCOO and presumably HCOOO). Alternatively, free electron attachment to any of these species is also possible. The negative ions so formed should also be thought of as bases (e.g. OH^- is a strong base, O_2^- a weak one). They can chemically ionize other species to form negative ions by proton abstraction from neutral acids present in the reaction zone (CH_3OH, possibly H_2O_2, HCOOH and perhaps the pair of peroxidic acids HCOOO and HCOOOH). Thus, the negative ions provide some evidence, albeit inconclusive, for the presence of peroxidic compounds in the flame. Clustering or three-body association reactions account for the other negative ions observed.

In many respects, the ion chemistry is very similar to that observed for an analogous fuel-lean methane—oxygen flame. This is particularly true downstream for both positive and negative ions. However, the combustion path leading to formic acid is favoured in the methanol flame compared with methane, probably stemming from the initial steps in the combustion of the oxygen-containing fuel molecule.

ACKNOWLEDGEMENTS

We wish to thank Thornton Research Centre, Shell Research Limited, Chester, England for the calculation of the adiabatic flame temperature and equilibrium burnt gas composition. Support of this work by the National Research Council of Canada under Grant Numbers A1604 (J.M.G.) and A6258 (D.K.B.) is acknowledged.

REFERENCES

1 M. Wayman, New Opportunities for Fuel from Biological Processes, Chemistry in Canada, November 1977, p. 26.
2 A.L. Hammond, Science, 195 (1977) 564.
3 J.M. Goodings, D.K. Bohme and Chun-Wai Ng, Combust. Flame, submitted.
4 J.M. Goodings, D.K. Bohme and Chun-Wai Ng, Combust. Flame, submitted.
5 J.M. Goodings, D.K. Bohme and T.M. Sugden, Sixteenth Symposium (International) on Combustion, The Combustion Institute, Pittsburgh, 1977, p. 891.
6 D.K. Bohme, J.M. Goodings and Chun-Wai Ng, Int. J. Mass Spectrom. Ion Phys., 24 (1977) 335.
7 D.F. Cooke, M.G. Dodson and A. Williams, Combust. Flame, 16 (1971) 233.
8 E. de Wilde and A. van Tiggelen, Bull. Soc. Chim. Belg., 77 (1968) 67.
9 H.T. Henderson and G.R. Hill, J. Phys. Chem., 60 (1956) 874.
10 W.H. Wiser and G.R. Hill, Fifth Symposium (International) on Combustion, Williams and Wilkins, Baltimore, 1955, p. 553.
11 D.R. Stull and H. Prophet et al., JANAF Thermochemical Tables, 2nd edn., NSRDS-NBS 37, U.S. Government Printing Office, 1971; M.W. Chase, J.L. Curnutt, A.T. Hu, H. Prophet, A.N. Syverud and L.C. Walker, JANAF Thermochemical Tables, 1974 Suppl., J. Phys. Chem. Ref. Data, 3 (1974) 311; M.W. Chase, J.L. Curnutt, H. Prophet, R.A. McDonald and A.N. Syverud, JANAF Thermochemical Tables, 1975 Suppl., J. Phys. Chem. Ref. Data, 4 (1975) 1.
12 E.M. Bulewicz and P.J. Padley, Ninth Symposium (International) on Combustion, Academic Press, New York, 1963, p. 638.
13 K.N. Bascombe, J.A. Green and T.M. Sugden, Advan. Mass Spectrom., 2 (1962) 66.
14 H.F. Calcote, Eighth Symposium (International) on Combustion, Williams and Wilkins, Baltimore, 1962, p. 184.
15 J.N. Bradley and D.A. Durden, Combust. Flame, (1972) 452.
16 A.G. Gaydon and H.G. Wolfhard, Third Symposium on Combustion, Flame and Explosion Phenomena, Williams and Wilkins, Baltimore, 1949, p. 504.
17 W.H. Wiser and G.R. Hill, Fifth Symposium (International) on Combustion, Reinhold, New York, 1955, p. 553.
18 K.M. Bell and C.F.H. Tipper, Proc. R. Soc., Ser. A, 238 (1956) 256.
19 D.J. Dixon and G. Skirrow, in G.H. Bamford and C.F.H. Tipper (Eds.), Comprehensive Chemical Kinetics, Vol. 17, Elsevier, Amsterdam, 1977, p. 369.
20 J.F. Griffiths and G. Skirrow, Oxid. Combust. Rev., 3 (1968) 47.
21 B. Lewis and G. von Elbe, Combustion, Flames and Explosions of Gases, 2nd edn., Academic Press, New York, 1961, p. 90.
22 J.M. Hay and K. Hessam, Combust. Flame, 16 (1971) 237.
23 D. Smith and N.G. Adams, Int. J. Mass Spectrom. Ion Phys., 23 (1977) 123.
24 P.M. Guyon, W.A. Chupka and J. Berkowitz, J. Chem. Phys., 64 (1976) 1419.
25 W.T. Huntress, Jr., Astrophys. J., Suppl. Ser., 33 (1977) 495.
26 N.G. Adams and D. Smith, Chem. Phys. Lett., 54 (1978) 530.
27 A.N. Hayhurst and N.R. Telford, J. Chem. Soc. Faraday Trans. I, 70 (1974) 1999.
28 S.D. Tanner, G.I. MacKay, A.C. Hopkinson and D.K. Bohme, Int. J. Mass Spectrom. Ion Phys., in press.
29 J. Long and B. Munson, J. Am. Chem. Soc., 95 (1973) 2427.
30 F.C. Fehsenfeld and E.E. Ferguson, J. Chem. Phys., 61 (1974) 3181.